

# Mutations in *SNX14* Cause a Distinctive Autosomal-Recessive Cerebellar Ataxia and Intellectual Disability Syndrome

Anna C. Thomas,<sup>1,14</sup> Hywel Williams,<sup>1,2,14</sup> N ria Set -Salvia,<sup>1,14</sup> Chiara Bacchelli,<sup>1,2</sup> Dagan Jenkins,<sup>1</sup> Mary O’Sullivan,<sup>1</sup> Konstantinos Mengrelis,<sup>1</sup> Miho Ishida,<sup>1</sup> Louise O’caka,<sup>1,2</sup> Estelle Chanudet,<sup>1,2</sup> Chela James,<sup>1,2</sup> Francesco Lescai,<sup>1,2,3</sup> Glenn Anderson,<sup>4</sup> Deborah Morrogh,<sup>5</sup> Mina Ryten,<sup>6,7</sup> Andrew J. Duncan,<sup>1</sup> Yun Jin Pai,<sup>8</sup> Jorge M. Saraiva,<sup>9,10</sup> Fabiana Ramos,<sup>9</sup> Bernadette Farren,<sup>11</sup> Dawn Saunders,<sup>12</sup> Bertrand Vernay,<sup>8</sup> Paul Gissen,<sup>1</sup> Anna Straatmaan-Iwanowska,<sup>1</sup> Frank Baas,<sup>13</sup> Nicholas W. Wood,<sup>6</sup> Joshua Hersheson,<sup>6</sup> Henry Houlden,<sup>6</sup> Jane Hurst,<sup>11</sup> Richard Scott,<sup>11</sup> Maria Bitner-Glindzic,<sup>1,11</sup> Gudrun E. Moore,<sup>1</sup> S rgio B. Sousa,<sup>1,9,15,\*</sup> and Philip Stanier<sup>1,15,\*</sup>

Intellectual disability and cerebellar atrophy occur together in a large number of genetic conditions and are frequently associated with microcephaly and/or epilepsy. Here we report the identification of causal mutations in Sorting Nexin 14 (*SNX14*) found in seven affected individuals from three unrelated consanguineous families who presented with recessively inherited moderate-severe intellectual disability, cerebellar ataxia, early-onset cerebellar atrophy, sensorineural hearing loss, and the distinctive association of progressively coarsening facial features, relative macrocephaly, and the absence of seizures. We used homozygosity mapping and whole-exome sequencing to identify a homozygous nonsense mutation and an in-frame multiexon deletion in two families. A homozygous splice site mutation was identified by Sanger sequencing of *SNX14* in a third family, selected purely by phenotypic similarity. This discovery confirms that these characteristic features represent a distinct and recognizable syndrome. *SNX14* encodes a cellular protein containing Phox (PX) and regulator of G protein signaling (RGS) domains. Weighted gene coexpression network analysis predicts that *SNX14* is highly coexpressed with genes involved in cellular protein metabolism and vesicle-mediated transport. All three mutations either directly affected the PX domain or diminished *SNX14* levels, implicating a loss of normal cellular function. This manifested as increased cytoplasmic vacuolation as observed in cultured fibroblasts. Our findings indicate an essential role for *SNX14* in neural development and function, particularly in development and maturation of the cerebellum.

Intellectual disability (ID) syndromes with a small cerebellum constitute a clinically and genetically heterogeneous group of neurological disorders for which the underlying molecular etiology is diverse and established in only a small subset. Several different cellular mechanisms have been implicated including mutations in *SIL1*, coding for an endoplasmic reticulum resident cochaperone, which cause Marinesco-Sjogren syndrome (MSS [MIM 248800]);<sup>1</sup> sialic acid disorders such as Salla disease (MIM 604369);<sup>2</sup> disorders of peroxisome biogenesis in atypical Refsum disease (MIM 614879);<sup>3</sup> congenital disorders of glycosylation, especially type 1a caused by mutations in *PMM2* (MIM 212065);<sup>4</sup> and the X-linked ID-small cerebellum syndrome caused by mutations in *OPHN1* (MIM 300486), a Rho-GTPase-activating protein (GAP).<sup>5</sup> Related phenotypes include the group designated as pontocerebellar hypoplasias,<sup>6</sup> within which causal mutations have been found in

a number of genes involved in tRNA biogenesis (including *RARS2* [MIM 611523], *TSEN54* [MIM 225753], *TSEN34* [MIM 612390], *TSEN2* [MIM 612389], and *CLP1* [MIM 615803]),<sup>6–10</sup> in rRNA processing (the exosomal genes *EXOSC3* [MIM 614678] and *EXOSC8* [MIM 606019]),<sup>11,12</sup> and another (*CHMP1A* [MIM 614961]), with a dual role in protein sorting at the endosome and chromatin modification at the nucleus.<sup>13</sup> Other cellular processes include synaptic and cell junction function (*CASK* [MIM 300749]),<sup>14</sup> cell cycle progression, and cell division (the serine-threonine kinase *VRK1* [MIM 607596]).<sup>15</sup> At the biochemical level, it is not clear how disruption of many of these genes leads to hindbrain hypoplasia or atrophy. The classification and diagnostic approach of cerebellar disease associated with ID in childhood is complex and challenging, often depending on the careful identification and assessment of neuroradiological and other clinical findings.<sup>15–18</sup>

<sup>1</sup>Genetics and Genomic Medicine, UCL Institute of Child Health, London WC1N 1EH, UK; <sup>2</sup>Centre for Translational Omics-GOSgene, UCL Institute of Child Health, London WC1N 1EH, UK; <sup>3</sup>Department of Biomedicine, Aarhus University, 8000 Aarhus, Denmark; <sup>4</sup>Histopathology Department, Great Ormond Street Hospital, London WC1N 3JH, UK; <sup>5</sup>NE Thames Regional Genetics Laboratory Service, London WC1N 3BH, UK; <sup>6</sup>UCL Institute of Neurology, London WC1N 3BG, UK; <sup>7</sup>Department of Clinical Genetics, Guy’s Hospital, London SE1 9RT, UK; <sup>8</sup>Developmental Biology and Cancer, UCL Institute of Child Health, London WC1N 1EH, UK; <sup>9</sup>Servi o de Gen tica M dica, Hospital Pedi trico, Centro Hospitalar e Universit rio de Coimbra, 3000-602 Coimbra, Portugal; <sup>10</sup>University Clinic of Pediatrics, Faculty of Medicine, University of Coimbra, 3000-602 Coimbra, Portugal; <sup>11</sup>Clinical Genetics, Great Ormond Street Hospital, London WC1N 3JH, UK; <sup>12</sup>Radiology, Great Ormond Street Hospital, London WC1N 3JH, UK; <sup>13</sup>Department of Genome Analysis, Academic Medical Center, University of Amsterdam, 1105AZ Amsterdam, the Netherlands

<sup>14</sup>These authors contributed equally to this work

<sup>15</sup>These authors contributed equally to this work

\*Correspondence: sbsousa@chc.min-saude.pt (S.B.S.), p.stanier@ucl.ac.uk (P.S.)

<http://dx.doi.org/10.1016/j.ajhg.2014.10.007>.  2014 The Authors

This is an open access article under the CC BY license (<http://creativecommons.org/licenses/by/3.0/>).



**Figure 1. Phenotype of Affected Individuals from the Three Families Presented**

Photographs and brain MRI scans from family 1 individual IV.3 aged 19 years (A) and 22 years (E); family 1 individual IV.6 aged 6 years (B, F) and 7 years (I, I'); family 2 individual V.1 aged 4.5 years (C, G, J, J'); family 3 individual III.2 aged 22 years (D, H) and 10 years (K, K'); and family 2 individual V.2 aged 9 months (L, L'). Notice the similar facial features mainly characterized by broad face, fullness of the upper eyelid, broad nasal base and slight underdevelopment of the alae, broad and long philtrum, thick lower lip vermilion, and fifth finger brachycamptodactyly. In the first years of life, no neuroradiological anomalies were observed in affected individuals, as depicted here by the normal T1-weighted mid-sagittal (L) and coronal (L') MRI sections, which have not yet been repeated for this individual. MRI images performed for other individuals during infancy are unavailable but were reported to be normal. At older ages, affected individuals have a small cerebellum with thin folia and enlarged fissures, suggestive of global cerebellar atrophy as shown here in the T1-weighted MRI images from three of the children, one from each family (mid-sagittal sections I–K; coronal sections I'–K'). The pons appear small but in comparison are well preserved.

We recently described an autosomal-recessive condition in a consanguineous Portuguese family (family 1) in which two sisters (Figures 1 and 2A) share a similar phenotype, characterized by severe cerebellar ataxia, severe intellectual disability (ID), absent speech, coarse facial features, relative macrocephaly, brachycamptodactyly of fifth fingers, and early-onset cerebellar atrophy (Table 1).<sup>21</sup> To perform ge-

netic analysis aimed at identifying the causal mutation, informed consents were obtained for all of the parents, probands, and siblings according to protocols approved by the ethical review committees at Great Ormond Street Hospital and Coimbra Hospital Centre. Specific parental consent was also given for the use of all of the clinical data and facial photographs included in this manuscript. The family was

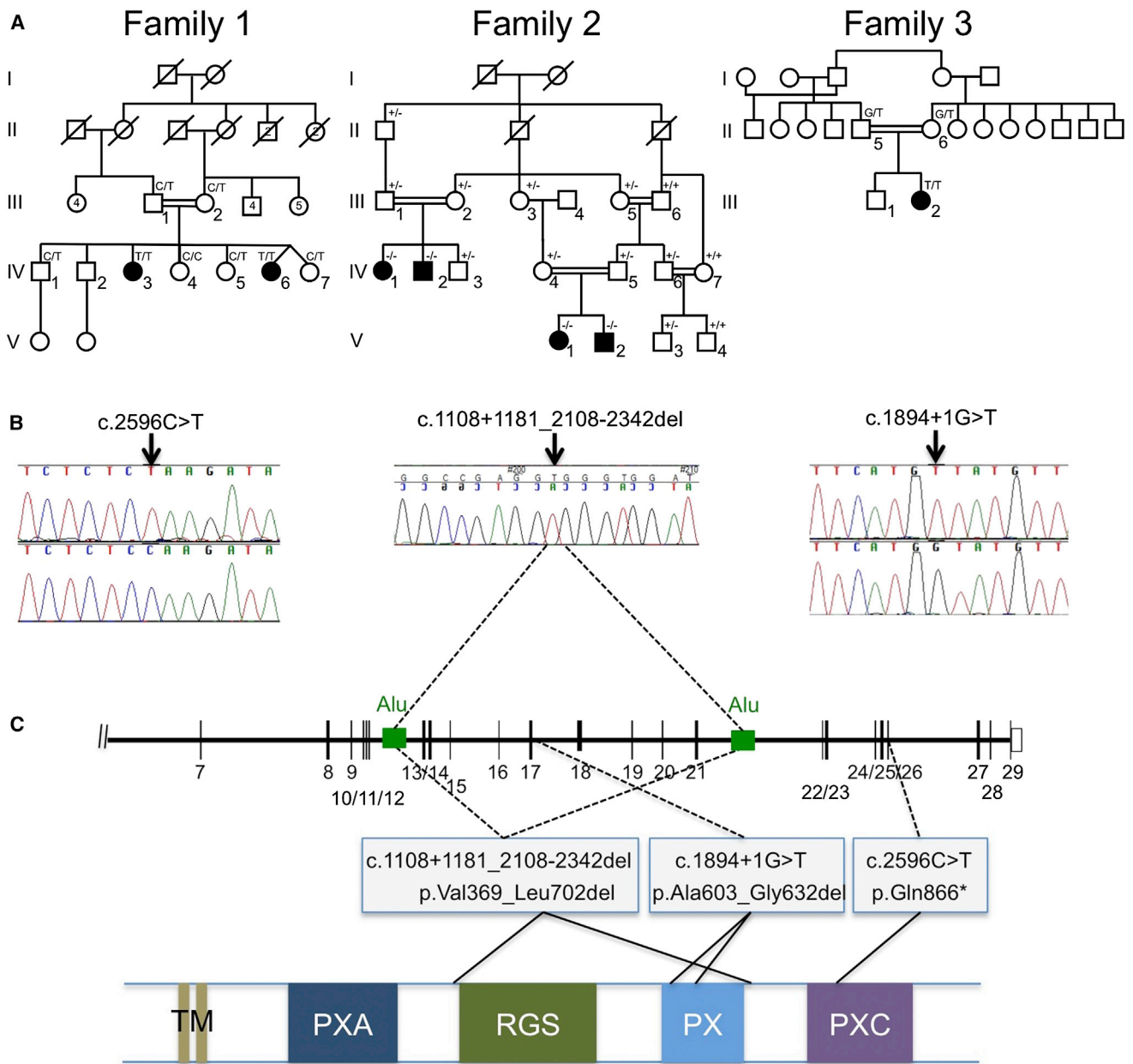


**Figure 2. Identification of *SNX14* Mutations in Three Affected Families**

(A) Pedigrees of the three families showing genotypes in tested individuals.

(B) Sequence traces for families 1 and 3 show point mutations in genomic DNA (top trace, mutant; bottom trace, wild-type). For family 2, the sequence trace spans the deletion breakpoint, in genomic DNA, and indicates the location of the breakpoints within two *Alu* repeats in the schematic diagram of the *SNX14* locus shown in (C) (see also Figure S1 for further details).

(C) Schematic representation of part of the *SNX14* genomic locus (top) and the *SNX14* protein (bottom) indicating the location and effect of the mutations detected in the three families. The protein consists of two predicted transmembrane domains (TM) at the N terminus, followed by the PXA domain, RGS domain, conserved PX phosphoinositide binding domain, and PXC domain situated toward the C terminus. The deletion in family 2 is predicted to remove the RGS and PX domains, whereas the splice site mutation in family 3 removes part of the PX domain.

then investigated by first delineating regions of shared homozygosity followed by whole-exome sequencing to identify variants in the implicated regions. Homozygosity mapping was performed on the two parents (III.1 and III.2), two affected siblings (IV.3 and IV.6), and four unaffected siblings (IV.1, IV.4, IV.5, and IV.7) using the Infinium HD HumanCytosNP-12 BeadChip (Illumina). This revealed 20 candidate

regions spanning a total of 35,846,704 bp, which contained 450 RefSeq and 886 UCSC transcripts (Table S1 available online). Haplotype analysis of the SNP data defined the largest homozygous region of ~18 Mb on 6q13-q14 (hg19; chr6: 70,500,118–88,497,536). Exome sequencing of the proband (IV.3) from family 1 was performed using Agilent SureSelect v.4 and Illumina TruSeq. Enriched libraries were

**Table 1. Clinical Findings in the Affected Individuals**

Mutation in <i>SNX14</i> (RefSeq NM_153816.3)	Family 1		Family 2				Family 3	Total
	homoz p.Gln866* (c.2596C>T)		homoz p.Val369_Leu702del (c.1108+1181_2108–2342del)			homoz p.Ala603_Leu632del (c.1894+1G>A)		
Subject ID	IV.3	IV.6	IV.1	IV.2	V.1	V.2	III.2	
Sex	F	F	F	M	F	M	F	5F, 2M
Present age (years)	26	14	32	16	10	3	23	
<b>Growth at Birth<sup>a</sup></b>								
Gestational age (weeks)	40	34 (twin)	U	U	40	40	U	
Length, cm (centile)	49 (50 <sup>th</sup> )	42 (10 <sup>th</sup> )	U	U	U	U	U	
Weight, g (centile)	3,600 (50 <sup>th</sup> )	2,100 (25 <sup>th</sup> )	U	U	2,650 (3–10 <sup>th</sup> )	2,800 (10–25 <sup>th</sup> )	U	
Head circumference, cm (centile)	35.5 (50 <sup>th</sup> )	32 (50 <sup>th</sup> )	U	U	U	35.5 (90 <sup>th</sup> )	U	
<b>Growth, Postnatal<sup>a</sup></b>								
Age (years)	22	14.5	29	14	6.7	1.0	22	
Height, cm (centile)	155 (10 <sup>th</sup> )	140 (<3 <sup>rd</sup> )	U	U	(91 <sup>st</sup> )	76.1 (<75 <sup>th</sup> )	157.7 (9–25 <sup>th</sup> )	
Head circumference (centile)	56.4 (75–90 <sup>th</sup> )	57.5 (90–97 <sup>th</sup> )	59 (>97 <sup>th</sup> )	55 (50 <sup>th</sup> )	55 (>97 <sup>th</sup> )	49.5 (97 <sup>th</sup> )	56.5 (75–90 <sup>th</sup> )	
<b>Neurodevelopment</b>								
Intellectual disability	severe	severe	severe	severe	severe	NA	moderate	
Speech (1 <sup>st</sup> words, years)	absent	sev impaired (13)	absent	absent	absent	absent	impaired (3)	5/7
Hypotonia	+	+	-	+	+	+	+	6/7
Sitting (age, months)	18	16	very late	>36	8	>12	12	18 <sup>b</sup>
Walking with help (age, months)	+ (24)	+ (20)	crawls	crawls	+ (24)	-	+ (18) <sup>c</sup>	4/7
Ataxia	+	+	wheelchair	wheelchair	+	NA	+	5/6
Talipes equino-varum	+	+	+	U	-	-	-	3/6
Hypo/areflexia	+	+	+	+	-	NA	+	5/6
<b>Craniofacial Features</b>								
Coarse features	+	+	+	+	+	+	+	7/7
Short palpebral fissures	+	+	+	+	+	+	-	6/7
Fullness of the upper eyelid	+	+	+	+	+	+	-	6/7
Broad/bulbous nose	+	+	+	+	+	+	+	7/7
Broad deep long philtrum	+	+	+	+	+	+	-	6/7
Thick lip vermilions (upper + lower)	+	+	+	+	+	+	+ (lower)	7/7
<b>Skeleton and Limbs</b>								
Scoliosis/kyphosis	-	-	+	+	-	-	-	2/7
Brachy/camptodactyly of 5th fingers	+	+	+	+	+	-	+	6/7
Short and broad finger/toes	+	+	+	+	+	+	(+)	7/7
Elbow motion limitation	+	+	U	-	-	-	+	3/6
Hearing loss	SN	+	-	SN	SN	-	SN	5/7

(Continued on next page)

**Table 1. Continued**

Mutation in <i>SNX14</i> (RefSeq NM_153816.3)	Family 1		Family 2			Family 3		Total
	homoz p.Gln866* (c.2596C>T)	MRI	MRI	CT	MRI	MRI	MRI	
Brain Imaging								
Age at last evaluation	20 years	7 years	U	10 months	4.5 years	9 months	10 years	
Cerebellar atrophy	+ P	+ P	+	–	+ P	–	+ P	5/7
Pontine thinning	+	–	U	–	+	–	(+)	4/7

Abbreviations and symbols are as follows: +, positive; –, negative/normal; U, data unknown; P, progressive: i.e., two or more sequential scans showed development/progression of the cerebellar atrophy; SN, sensorineural, moderate-severe, bilateral; NA, not applicable.

<sup>a</sup>Growth measurements: For the Turkish individuals, the charts used for head circumference measurements were described by Evereklioglu et al.<sup>19</sup> and Elmali et al.<sup>20</sup> The Portuguese individuals were compared to national charts except for head circumference >36 cm, or where not available, the charts described by Evereklioglu et al.<sup>19</sup> were used.

<sup>b</sup>Median for sitting age.

<sup>c</sup>Subject III.2 from family 3 was the only individual who progressed to independent ambulation, which was reached at age 3 years.

sequenced on an Illumina HiSeq2000 by Perkin Elmer, resulting in a mean of 66× read depth with 68% of targeted bases covered at least 1×. We sequenced one sample per lane, aligning the resulting reads to the reference genome build GRCh37/hg19 using Burrows-Wheeler Aligner (v.0.5.7) and for variant calling we applied GATK base quality score recalibration,<sup>22</sup> INDEL realignment, and duplicate removal and performed SNP and INDEL discovery and genotyping across all samples simultaneously using variant quality score recalibration.<sup>23</sup> Variant annotation and interpretation analysis was generated through the use of Ingenuity Variant Analysis software v.3.0.20140422 from Ingenuity Systems. With the use of filters outlined in Table S2 designed to pinpoint novel or rare homozygous damaging variants, we reduced the number of variants from an initial 159,274 genome wide, to a single likely causal mutation. This was a unique, homozygous nonsense variant (c.2596C>T [p.Gln866\*]) within *SNX14*, located at 6q14.3, which is within the largest autozygous interval (Figures 2B and 2C; Table S3). Sanger sequencing using Big Dye Terminator v.1.1 (Life Technologies) on an ABI 3730 sequencer (Applied Biosystems) confirmed that the mutation was homozygous in both affected sisters and segregated as an autosomal recessive, being heterozygous in both parents and absent or heterozygous in four unaffected siblings (Figure 2A). The *SNX14* locus generates two transcripts consisting of either 29 exons encoding the 946 amino acid isoform a (RefSeq NM\_153816.2) or 26 exons, lacking exons 14, 23, and 24, encoding a shorter protein of 893 amino acids known as isoform b (RefSeq NM\_020468.3). Both isoforms share the same four conserved domains: the PX (phosphoinositide binding, Phox homology), RGS (regulator of G protein signaling), PXA (PX-associated domain A), and PXC (PX-associated domain C) (Figure 2C). The c.2596C>T mutation was identified within an exon that codes for both transcripts (exon 26, based on the longer transcript) and was predicted to result in a protein truncation that would either remove the last 81 amino acids, including part of the PXC

domain or, alternatively, trigger nonsense-mediated decay (Figure 2C).

We identified a Turkish consanguineous family (family 2) with four affected individuals sharing similar clinical features to family 1 (Table 1; Figures 1 and 2A). SNP genotyping (as above), revealed 11 regions of homozygosity shared between all three of the affected individuals available at the time of mapping (IV.1, IV.2, and V.1), with the largest (8,056,114 bp) including the interval containing *SNX14* in 6q14.3, being the only autozygous region in common with family 1 (Table S1). Individual V.1 underwent exome sequencing at Dasman Diabetes Institute (Kuwait City, Kuwait) using methodologies as described for family 1, with 89% of target bases covered at least 1× with an average depth of 33× per base. Using the same filtering parameters as those for family 1, we were able to reduce the number of variants from 199,920 to 18 (Table S2). As examination of these failed to identify any of these within the regions of shared homozygosity, we decided to look in more detail at *SNX14*. Specifically, we viewed the reads across *SNX14* using Integrative Genomics Viewer (IGV) software (Broad Institute),<sup>24</sup> which revealed a homozygous deletion of 9 consecutive exons from exon 13 to 21 (with respect to isoform a) (Figure S1A and Table S4), while all DNAs sequenced at the same time from unaffected subjects had good read depth for this interval (Figure S1A). The deletion was confirmed, first noting the lack of PCR amplification of individual exons from genomic DNAs, then by testing a series of primers flanking the approximate breakpoint position (Figure S1B). The latter strategy allowed determination of the precise sequence of the junction fragment. The deletion most likely occurred as a consequence of illegitimate recombination between two *Alu*-repeat sequences found in intron 12 and intron 21. This resulted in a deletion spanning 25,640 bases, described as c.1108+1181\_2108–2342del with reference to isoform a cDNA or hg19 coordinates chr6: 86,255,692–86,230,052 (Figure S1C). In addition, Affymetrix CytoScan 750K array analysis of the youngest affected individual (V.2) revealed a

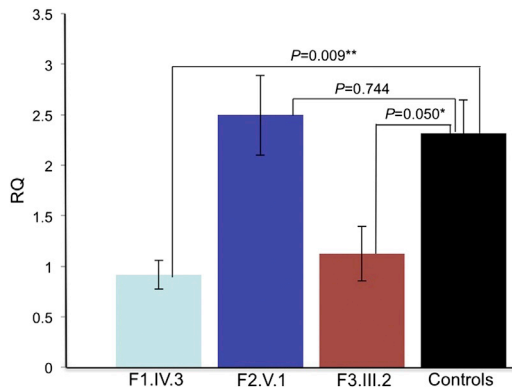


**Figure 3. SNX14 RNA Expression in Fibroblasts from Affected and Control Individuals**

qRT-PCR showing relative quantification (RQ  $\Delta\Delta\text{CT}$  method) of *SNX14* expression in affected fibroblasts samples from each family compared with controls. Both *GAPDH* and *HPRT1* were used as combined endogenous controls, with RQ calculated using StepOne analysis software v.2.1 (Life Technologies). Each experiment was biologically replicated three times with each sample analyzed in triplicate. Using a two-tailed t test, family 1 individual IV.3 shows a 60% decrease in expression compared to combined controls, where fibroblasts from five different control individuals have been analyzed (N = 5), \*\*p = 0.009. Family 3 individual III.2 shows a 51% drop in expression compared to controls, \*p = 0.05. However, family 2 individual V.1 shows no significant difference in expression compared to controls, p = 0.74. Error bars correspond to mean  $\pm$  SEM.

homozygous deletion spanning five consecutive probes within *SNX14*, corresponding to the interval described above (Figure S2). Sanger sequencing of cDNA synthesized from fibroblast mRNA (V.1) confirmed that there was in-frame splicing between exon 12 and exon 22 (Figure S1D), which is predicted to remove 334 amino acids (p.Val369\_Leu702del) from the full-length protein, including the entire RGS and PX domains (Figure 2C). We genotyped all of the available family members using a PCR-based approach to confirm segregation of the deletion. This revealed that only the four affected individuals were homozygous for the deletion, although eight unaffected individuals were heterozygous and three were homozygous for the reference allele (Figure 2A).

We next searched the Great Ormond Street Hospital Clinical Genetics records to identify affected individuals based solely on similar features. We performed text searches of the electronic medical records of all children known to the Clinical Genetics department using the terms “pontocerebellar hypoplasia,” “cerebellar hypoplasia,” OR “cerebellar atrophy” AND “hearing loss” and manually examined all sets of notes and clinical photographs, excluding all affected individuals with an alternative diagnosis or with microcephaly. This strategy identified family 2 (above) and a single further individual in an unrelated Turkish consanguineous family (family 3) among more than 50 case subjects matching the pontocerebellar or cerebellar search terms. The individual III.1 from family 3 (Figure 2A) had cerebellar ataxia, sensorineural hearing loss, slightly coarse facial features, relative macro-

cephaly, and bilateral fifth finger camptodactyly but generally had milder features than the other affected individuals in terms of the radiological degree of cerebellar atrophy and her motor, intellectual, and speech development (Table 1). Sanger sequencing of *SNX14* exons and exon-intron boundaries in III.1 identified a homozygous canonical splice site mutation (c.1894+1G>A), which was heterozygous in both parents (Figure 2A). Using mRNA isolated from peripheral blood lymphocytes, we confirmed in-frame splicing of exon 18 to exon 20 (isoform a), completely skipping exon 19 (Figure S3). This was predicted to result in the deletion of 30 amino acids (p.Ala603\_Gly632del) from within the PX domain (Figure 2C).

Using fibroblast cDNA, we compared mutant and wild-type transcript levels using quantitative RT-PCR with Power SYBR green PCR Master Mix on StepOnePlus Real-Time PCR Systems (Life Technologies). Compared to controls, we noted significantly reduced levels of expression in families 1 and 3, whereas levels in family 2 were similar (Figure 3). To investigate protein levels, *SNX14* was analyzed by immunoblotting (Figure S4). A single band of ~110 kDa was reproducibly obtained in control fibroblasts, but no band was detected in either family 1:IV.6 or 2:V.1. For family 1:IV.6, only a low level of mRNA was present, and this may produce an unstable or subdetectable level of protein. This also ties in with the possibility of activation of the nonsense-mediated decay pathway. For family 2:V.1, the deletion removes 112 of the 131 amino acid peptides used to raise the anti-*SNX14* antibody. Therefore, it is conceivable that a truncated protein is present but not detectable with this assay. For family 3:III.2, a protein of slightly lower molecular weight (~107 kDa) is detected, approximating to the loss of amino acids due to skipping of exon 19. Collectively, the mutation data are supportive of a loss of normal biological function for *SNX14*.

Therefore, we identified a total of seven affected individuals from three unrelated families who share a distinct rare syndrome resulting from *SNX14* mutations. Neither point mutation was present in the NHLBI-ESP-EVS 4,870 exomes or in our internal database of 358 exomes. The Database of Genomic Variants lists 13 unaffected individuals who are heterozygous for 7 different but overlapping microdeletions of ~31–130 kb (n = 1/2,026; 1/2,026; 7/2026; 1/1,557; 1/443; 1/17,421; 1/17,421)<sup>25–28</sup> and a single 40 kb microduplication (n = 1/2,026),<sup>25</sup> all involving parts of the *SNX14* locus. However, a review of 4,500 GOSH children screened using the Affymetrix 750K array did not identify any further individuals, other than from family 2, who carry deletions or duplications that included *SNX14*.

Only five individuals with microdeletions involving *SNX14* are well described in the literature.<sup>29–32</sup> Two of these are included in DECIPHER, which lists seven individuals with intellectual disability and other various defects who have large (~5 Mb) heterozygous deletions, and a

further two with duplications that encompass *SNX14* and other nearby genes. Of these, only the two unrelated individuals described by Wentzel et al.,<sup>31</sup> who have large interstitial deletions (8.7 Mb and 4.5 Mb) containing *SNX14* and three neighboring genes, have some phenotypic similarity to our affected individuals. In particular this includes the presence of ID, similar facial dysmorphic features, hearing loss, and macrocephaly. Additionally, one of these individuals had camptodactyly and limited movement of the elbows. None of them were reported to have cerebellar atrophy or ataxia, but both of them had walking difficulties and one was reported to have dyspraxia. Currently, we cannot exclude the presence of a second, *SNX14*-specific point mutation on the non-CNV-carrying chromosome in these cases.

In an attempt to further extend the phenotypic spectrum associated with *SNX14* mutations, we investigated whole-exome sequencing data obtained for a series of 36 individuals with idiopathic pontocerebellar hypoplasia, and 168 from dominant and recessive families with idiopathic cerebellar ataxia, of which 138 were recessive/early onset or no family history. However, no likely causal variants or CNVs affecting *SNX14* were identified. These data suggest that autosomal-recessive *SNX14* mutations are associated with a narrow clinical spectrum. The presence of coarse faces and the absence of microcephaly and epilepsy are distinctive features within this group of conditions, confirming our findings reported in the description of the first family.<sup>21</sup> Additionally, sensorineural hearing loss and camptodactyly of fifth fingers seem also to be prevalent (Table 1). Nevertheless, it should be noted that clinical recognition is challenging in infants because dysmorphic features, cerebellar involvement, ID, speech impairment, and ataxia are progressive and absent at an early age. Neuroradiological scans performed in the first years of life appeared normal but later were characterized by a globally small cerebellum (Table 1, Figure 1). Both the hemispheres and vermis are affected and there is separation of the folia indicating atrophy rather than hypoplasia (Figure 1). Evidence for slight pontine thinning was seen in older patients. This phenotype is significantly different from the pontocerebellar hypoplasias group of conditions, which are usually more severe, with prenatal-onset hypoplasia/atrophy of cerebellum and pons, associated with progressive microcephaly and seizures.

*SNX14* is a member of the large family of sorting nexin proteins but it has only recently been investigated for its tissue distribution and cellular function. The earliest report describes *Snx14* mRNA expression using an in vitro motoneuron selection method.<sup>33</sup> Mice in this study were found to have the highest levels of *Snx14* mRNA expression at E12.5, restricted to neuronal lineages such as the spinal cord. Expression in the brain was seen in the ventral ventricular region, the floor plate, V (trigeminal) and VIII (vestibulocochlear) cranial ganglia, the sacculle of the inner ear, the developing pituitary gland, and eye. In general, mRNA distribution was described

as colocalizing with *Islet-1* expression, including *Islet-1*-positive motoneurons.<sup>33</sup> Furthermore, Northern blot analysis in different adult mouse tissues revealed *Snx14* expression in cerebellum and hippocampus and at much lower levels in cortex, muscle, liver, lung, and heart.<sup>33</sup>

We investigated *SNX14* mRNA expression in human fetal tissue using RT-PCR and found it to be ubiquitously present in all tissues analyzed, including heart, skin, brain, kidney, bone, liver, eye, and placenta (Figure S5). The Allen Brain Atlas reports in situ hybridization for the p56 mouse brain, where the highest levels of *Snx14* expression were found in the granule and Purkinje cell layers of the cerebellar cortex but also in the hippocampus (granule layers and dentate gyrus) and the piriform. This was supported by data from both the human UK Brain Expression Consortium (UKBEC) and the Human Brain Transcriptome database.<sup>34,35</sup> *SNX14* is expressed in all brain regions, with generally increasing levels during prenatal development and then plateauing. Interestingly, the pattern the cerebellum is the region where *SNX14* is most highly expressed and transcript levels continue to increase through postnatal life until adult (UKBEC data, Figure S6). Most recently, Huang et al.<sup>36</sup> described mouse *SNX14* levels as being high in brain, testis, and lung, similarly showing an increase in cerebellar levels from embryonic to postnatal stages (E16.5–p63). Despite a broadly distributed spatiotemporal pattern, which might suggest function in many tissues, high levels in the central nervous system and particularly cerebellum correspond to the described phenotype (with internal organs spared), particularly the cerebellar atrophy seen in affected individuals from all three families presented here.

To date there are 49 mammalian proteins known to contain a PX domain and the majority of these are classified as sorting nexin proteins.<sup>37</sup> The PX domain binds to phosphoinositides (PtdIns3P) on the cytoplasmic leaflets of various organelles and it defines both subcellular localization and function of different PX domain-containing proteins including endosomal sorting and trafficking.<sup>37</sup> Mutations in the p47<sup>phox</sup> subunit of NADPH oxidase are known to cause autosomal-recessive chronic granulomatous disease (MIM 233700),<sup>38</sup> whereas *SNX27* has been indirectly linked to synaptic dysfunction in Down syndrome through impaired transcriptional regulation,<sup>39</sup> and recently *SNX10* mutations have been demonstrated to cause a nonsyndromic autosomal-recessive form of osteopetrosis (MIM 615085), an osteoclast-related bone disease.<sup>40</sup>

Based on predicted domain structure, *SNX14* is classified within the PXA-RGS-PX-PXC subfamily along with *SNX13*, *SNX19*, and *SNX25*.<sup>41</sup> Like *SNX13*, *SNX14* also contains a putative double transmembrane domain including a short cytoplasmic leader sequence and an RGS domain, implying they share a similar function (Figure 2C). The RGS domain of *SNX13* can bind to and increase the GTPase activity of the G- $\alpha_s$  ( $G\alpha_s$ ) subunit of G-protein coupled receptors (GPCRs). Mediated by the PX

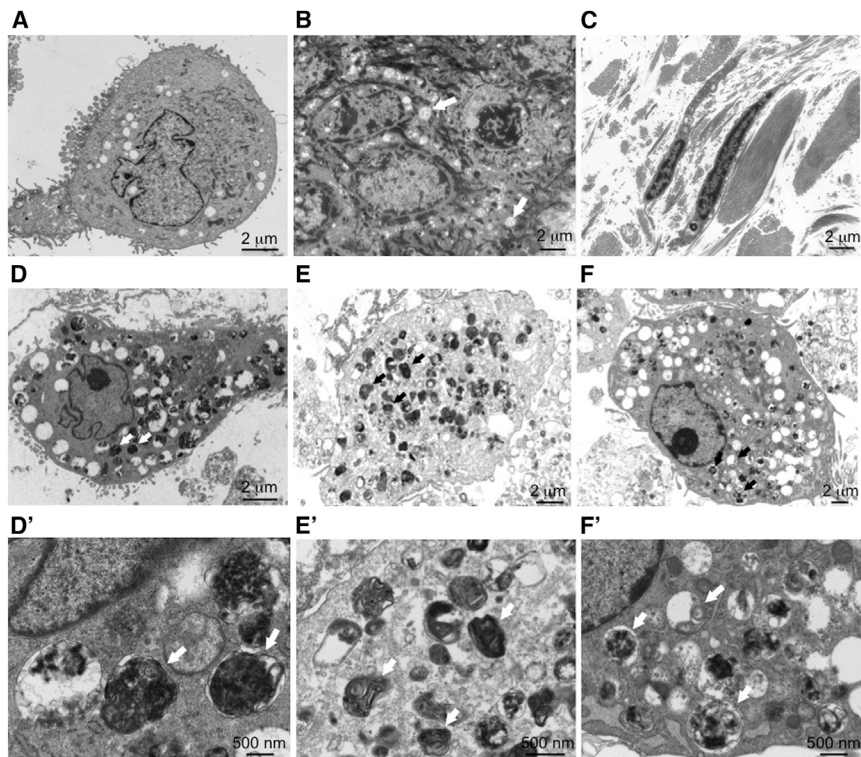


**Figure 4. Electron Micrographs of Skin Biopsy and Cultured Fibroblasts**

(A) Control cultured fibroblast at 800× magnification.

(B and C) Skin section from family 3 individual III.2 at 800× magnification.

(B) In the epidermis, there was mild hyperkeratosis with keratinocytes showing increased vacuolation, containing fine nonspecific granular material (arrows).

(C) In the dermis, collagen and elastic tissue had a normal appearance and distribution with infrequent vacuoles in the fibroblasts.

(D–F) Cultured fibroblasts from family 1 individual IV.6, family 2 individual V.1, and family 3 individual III.2, respectively, at 800× magnification. The cells showed numerous cytoplasmic vacuoles, often containing dense staining material suggestive of lipid degeneration. Same cells at 3,000× magnification shown in (D′)–(F′). Vacuoles contained granular material or multilamellar bodies or were empty (see white and black arrows for examples).

domain, this activity can occur at the endosome, allowing  $G\alpha_s$  signal attenuation at the interface with this protein sorting and degradation pathway.<sup>42,43</sup> Loss of functional SNX13 in the mouse resulted in dramatically altered endocytic/lysosomal compartmentalization in visceral yolk sac endoderm, with abnormal localization of several endocytic markers and with the appearance of abundant autophagic vacuoles.<sup>44</sup>

A role for SNX14 in endosomal sorting and the regulation of protein degradation is supported by recent analyses of the prenatal human brain transcriptome.<sup>45</sup> Weighted gene coexpression network analysis (WGCNA) was used to group genes expressed within mid-fetal human neocortex into modules in an unsupervised manner.<sup>46</sup> This approach is extremely useful in identifying modules of biologically related genes that are not just coexpressed, but coregulated.<sup>47</sup> This method was applied to predict that *SNX14* is highly coexpressed within a module (C25, black),<sup>45</sup> which is significantly enriched for genes involved in cellular protein metabolism (Gene ontology term GO:0044267~cellular protein metabolic process, Bonferroni-corrected  $p$  value =  $9.18 \times 10^{-5}$ ) and vesicle-mediated transport between the ER and Golgi (GO:0006888~ER to Golgi vesicle-mediated transport, Bonferroni-corrected  $p$  value =  $7.59 \times 10^{-4}$ ).

This prompted us to examine cellular ultrastructural morphology in skin biopsy material and fibroblast cell lines, using a JEOL 1400 transmission electron microscope (Figure 4). Compared to control samples, the skin biopsy showed an adequate epithelial layer with a moderate degree of hyperkeratosis and occasional apoptotic bodies.

Vacuoles with fine nonspecific granular material were identified in keratinocytes (Figure 4B). In the dermis, collagen and elastic tissue had a normal appearance and distribution. Fibroblasts demonstrated infrequent vacuoles with granular material and rare electron-dense laminated inclusions suggestive of lipid degeneration. No sweat glands were available for assessment and small myelinated and unmyelinated nerves were unremarkable. Next, we investigated ultrathin sections from cultured skin fibroblasts from one affected individual from each of the three families and control subjects. Affected fibroblasts were found to have frequent cytoplasmic vacuolation with electron-dense material of variable morphology including some with evidence of lamella structure as seen in multilamellar bodies (Figures 4D–4F). Interestingly, a proportion of fibroblasts from affected individuals but not control subjects immunostain positive for p62 in a granular pattern (Figure S7), which might suggest a defect in the autophagy pathway, as seen in many neurodegenerative and neurodevelopmental disorders.<sup>48</sup> Interestingly, cultured fibroblasts from individuals with MSS similarly contain numerous cytoplasmic electron-dense, sometimes multilamellar inclusion, bodies in both individuals with and without *SIL1* mutations.<sup>1</sup> MSS and the *SNX14* phenotype share the presence of ID, cerebellar atrophy, hypotonia, and ataxia. Therefore *SNX14* should be screened in MSS-like individuals not carrying an *SIL1* mutation, especially in those without microcephaly, cataracts, or myopathy (creatinine kinase levels were in the normal range for the four individuals tested who have *SNX14* mutations).



Zheng et al.<sup>44</sup> reported that heterozygous *Snx13*<sup>+/-</sup> mice do not have an obvious phenotype, whereas *Snx13*<sup>-/-</sup> mice die between E10.5 and E14.5. Mutants are small and have exencephaly and abnormal cephalic vascularization, presumably in response to defective nutrient uptake and transport, particularly in the yolk sac endoderm, which could account for embryonic developmental delay. *Snx14* knockdown studies using lentiviral shRNA, specifically in mouse cortical pyramidal neurons, were recently reported.<sup>36</sup> Despite incomplete (60%) knockdown, significantly reduced intrinsic excitability and synaptic function was recorded. The study of Huang et al.<sup>36</sup> also reported *Snx14* to be maternally imprinted but suggest that this might be mouse specific. Our data support this because unaffected heterozygous individuals inherit the mutation on either the maternal or paternal allele (Figure 2A).

In conclusion, in terms of a potential mechanism there is a compelling case for a role of SNX14 in synaptic transmission.<sup>40</sup> Synaptic dysfunction is well known to be implicated in neurodevelopmental disorders associated with ID<sup>49</sup> and this may underlie the pathogenesis of SNX14 mutations. Other genes coding RGS proteins, especially of the Rho GTPase family, cause ID syndromes and have a crucial role in synaptic structure/function.<sup>50</sup> Interestingly, a significant phenotypic overlap is seen with *OPHN1* encoding a Rho-GAP protein, in which mutations cause an X-linked form of syndromic ID typically associated with cerebellar abnormalities, dysmorphic (often coarse) facial features, and sometimes macrocephaly.<sup>5,50</sup> Overall, our results implicate an essential role for SNX14 with the breakdown and recycling of cellular components in human cerebellar development and maintenance.

### Supplemental Data

Supplemental Data include seven figures and four tables and can be found with this article online at <http://dx.doi.org/10.1016/j.ajhg.2014.10.007>.

### Acknowledgments

We would like to thank the families who contributed to this study. We would also like to thank the expert assistance of Kerra Pearce (UCL Genomics) for running the SNP genotyping arrays, Osama Alsmadi and Dinu Antony for exome sequencing at The Dasman Diabetes Institute Genome Centre (Kuwait City), and Manuela Grazina (Faculty of Medicine, University of Coimbra) and Biljana Lukovic (Chemical Pathology, Great Ormond Street Hospital for Children) for providing an affected individual's fibroblast culture. P.S. is supported by the Great Ormond Street Hospital Children's Charity. S.B.S. was supported by Fundação para a Ciência e Tecnologia (SFRH/BD/46778/2008). A.C.T. is a Wellbeing of Women Research Associate. G.E.M.'s Fetal Growth and Development research group is supported by Wellbeing of Women, MRC, Sparks and the National Institute for Health Research Biomedical Research Centre (NIHR BRC) at Great Ormond Street Hospital for Children NHS Foundation Trust, and UCL Institute of Child Health. E.B. is supported by the Joshua Deeth foundation. We thank the additional members of the GOSgene Scientific Advisory

Board (Philip Beales, Robert Kleta, Horia Stanesku, Nicholas Lench, Bobby Gaspar, Michael Hubank, and Elia Stupka). GOSgene is supported by the NIHR BRC at Great Ormond Street Hospital for Children NHS Foundation Trust and UCL Institute of Child Health. This report is independent research by the NIHR BRC Funding Scheme. The views expressed in this publication are those of the author(s) and not necessarily those of the NHS, the National Institute for Health Research, or the Department of Health.

Received: August 21, 2014

Accepted: October 13, 2014

Published: November 6, 2014

### Web Resources

The URLs for data presented herein are as follows:

1000 Genomes, <http://browser.1000genomes.org>  
Allen Mouse Brain Atlas, <http://mouse.brain-map.org>  
Database of Genomic Variants (DGV), <http://dgv.tcag.ca/dgv/app/home>  
dbSNP, <http://www.ncbi.nlm.nih.gov/projects/SNP/>  
Ingenuity Variant Analysis, <http://www.ingenuity.com/products/variant-analysis>  
NHLBI Exome Sequencing Project (ESP) Exome Variant Server, <http://evs.gs.washington.edu/EVS/>  
Online Mendelian Inheritance in Man (OMIM), <http://www.omim.org/>  
RefSeq, <http://www.ncbi.nlm.nih.gov/RefSeq>  
UCSC Genome Browser, <http://genome.ucsc.edu>

### References

1. Ezgu, F., Krejci, P., Li, S., de Sousa, C., Graham, J.M., Jr., Hansmann, I., He, W., Porpora, K., Wand, D., Wertenlecker, W., et al. (2014). Phenotype-genotype correlations in patients with Marinesco-Sjögren syndrome. *Clin. Genet.* *86*, 74–84.
2. Strehle, E.M. (2003). Sialic acid storage disease and related disorders. *Genet. Test.* *7*, 113–121.
3. Waterham, H.R., and Ebberink, M.S. (2012). Genetics and molecular basis of human peroxisome biogenesis disorders. *Biochim. Biophys. Acta* *1822*, 1430–1441.
4. Matthijs, G., Schollen, E., Pardon, E., Veiga-Da-Cunha, M., Jaeken, J., Cassiman, J.J., and Van Schaftingen, E. (1997). Mutations in *PMM2*, a phosphomannomutase gene on chromosome 16p13, in carbohydrate-deficient glycoprotein type I syndrome (Jaeken syndrome). *Nat. Genet.* *16*, 88–92.
5. Philip, N., Chabrol, B., Lossi, A.M., Cardoso, C., Guerrini, R., Dobyns, W.B., Raybaud, C., and Villard, L. (2003). Mutations in the oligophrenin-1 gene (*OPHN1*) cause X linked congenital cerebellar hypoplasia. *J. Med. Genet.* *40*, 441–446.
6. Namavar, Y., Chitayat, D., Barth, P.G., van Ruissen, F., de Wisel, M.B., Poll-The, B.T., Silver, R., and Baas, F. (2011). *TSEN54* mutations cause pontocerebellar hypoplasia type 5. *Eur. J. Hum. Genet.* *19*, 724–726.
7. Edvardson, S., Shaag, A., Kolesnikova, O., Gomori, J.M., Tarasov, I., Einbinder, T., Saada, A., and Elpeleg, O. (2007). Deleterious mutation in the mitochondrial arginyl-transfer RNA synthetase gene is associated with pontocerebellar hypoplasia. *Am. J. Hum. Genet.* *81*, 857–862.

8. Budde, B.S., Namavar, Y., Barth, P.G., Poll-The, B.T., Nürnberg, G., Becker, C., van Ruissen, F., Weterman, M.A., Fluiter, K., te Beek, E.T., et al. (2008). tRNA splicing endonuclease mutations cause pontocerebellar hypoplasia. *Nat. Genet.* *40*, 1113–1118.
9. Karaca, E., Weitzer, S., Pehlivan, D., Shiraishi, H., Gogakos, T., Hanada, T., Jhangiani, S.N., Wiszniewski, W., Withers, M., Campbell, I.M., et al.; Baylor Hopkins Center for Mendelian Genomics (2014). Human CLP1 mutations alter tRNA biogenesis, affecting both peripheral and central nervous system function. *Cell* *157*, 636–650.
10. Schaffer, A.E., Eggens, V.R., Caglayan, A.O., Reuter, M.S., Scott, E., Coufal, N.G., Silhavy, J.L., Xue, Y., Kayserili, H., Yasuno, K., et al. (2014). CLP1 founder mutation links tRNA splicing and maturation to cerebellar development and neurodegeneration. *Cell* *157*, 651–663.
11. Wan, J., Yourshaw, M., Mamsa, H., Rudnik-Schöneborn, S., Menezes, M.P., Hong, J.E., Leong, D.W., Senderek, J., Salman, M.S., Chitayat, D., et al. (2012). Mutations in the RNA exosome component gene EXOSC3 cause pontocerebellar hypoplasia and spinal motor neuron degeneration. *Nat. Genet.* *44*, 704–708.
12. Boczonadi, V., Müller, J.S., Pyle, A., Munkley, J., Dor, T., Quartararo, J., Ferrero, I., Karcagi, V., Giunta, M., Polvikoski, T., et al. (2014). EXOSC8 mutations alter mRNA metabolism and cause hypomyelination with spinal muscular atrophy and cerebellar hypoplasia. *Nat. Commun.* *5*, 4287.
13. Mochida, G.H., Ganesh, V.S., de Michelena, M.I., Dias, H., Atabay, K.D., Kathrein, K.L., Huang, H.T., Hill, R.S., Felie, J.M., Rakiec, D., et al. (2012). CHMP1A encodes an essential regulator of BMI1-INK4A in cerebellar development. *Nat. Genet.* *44*, 1260–1264.
14. Najm, J., Horn, D., Wimplinger, I., Golden, J.A., Chizhikov, V.V., Sudi, J., Christian, S.L., Ullmann, R., Kuechler, A., Haas, C.A., et al. (2008). Mutations of CASK cause an X-linked brain malformation phenotype with microcephaly and hypoplasia of the brainstem and cerebellum. *Nat. Genet.* *40*, 1065–1067.
15. Renbaum, P., Kellerman, E., Jaron, R., Geiger, D., Segel, R., Lee, M., King, M.C., and Levy-Lahad, E. (2009). Spinal muscular atrophy with pontocerebellar hypoplasia is caused by a mutation in the VRK1 gene. *Am. J. Hum. Genet.* *85*, 281–289.
16. D'Arrigo, S., Viganò, L., Grazia Bruzzone, M., Marzaroli, M., Nikas, I., Riva, D., and Pantaleoni, C. (2005). Diagnostic approach to cerebellar disease in children. *J. Child Neurol.* *20*, 859–866.
17. Anheim, M., Fleury, M., Monga, B., Laugel, V., Chaigne, D., Rodier, G., Ginglinger, E., Boulay, C., Courtois, S., Drouot, N., et al. (2010). Epidemiological, clinical, paraclinical and molecular study of a cohort of 102 patients affected with autosomal recessive progressive cerebellar ataxia from Alsace, Eastern France: implications for clinical management. *Neurogenetics* *11*, 1–12.
18. Poretti, A., Wolf, N.I., and Boltshauser, E. (2008). Differential diagnosis of cerebellar atrophy in childhood. *Eur. J. Paediatr. Neurol.* *12*, 155–167.
19. Evereklioglu, C., Doganay, S., Er, H., Gunduz, A., Tercan, M., Balat, A., and Cumurcu, T. (2002). Craniofacial anthropometry in a Turkish population. *Cleft Palate Craniofac. J.* *39*, 208–218.
20. Elmali, F., Altunay, C., Mazicioglu, M.M., Kondolot, M., Ozturk, A., and Kurtoglu, S. (2012). Head circumference growth reference charts for Turkish children aged 0–84 months. *Pediatr. Neurol.* *46*, 307–311.
21. Sousa, S.B., Ramos, F., Garcia, P., Pais, R.P., Paiva, C., Beales, P.L., Moore, G.E., Saraiva, J.M., and Hennekam, R.C.M. (2014). Intellectual disability, coarse face, relative macrocephaly, and cerebellar hypotrophy in two sisters. *Am. J. Med. Genet. A.* *164A*, 10–14.
22. McKenna, A., Hanna, M., Banks, E., Sivachenko, A., Cibulskis, K., Kernytzky, A., Garimella, K., Altshuler, D., Gabriel, S., Daly, M., and DePristo, M.A. (2010). The Genome Analysis Toolkit: a MapReduce framework for analyzing next-generation DNA sequencing data. *Genome Res.* *20*, 1297–1303.
23. DePristo, M.A., Banks, E., Poplin, R., Garimella, K.V., Maguire, J.R., Hartl, C., Philippakis, A.A., del Angel, G., Rivas, M.A., Hanna, M., et al. (2011). A framework for variation discovery and genotyping using next-generation DNA sequencing data. *Nat. Genet.* *43*, 491–498.
24. Thorvaldsdóttir, H., Robinson, J.T., and Mesirov, J.P. (2013). Integrative Genomics Viewer (IGV): high-performance genomics data visualization and exploration. *Brief. Bioinform.* *14*, 178–192.
25. Shaikh, T.H., Gai, X., Perin, J.C., Glessner, J.T., Xie, H., Murphy, K., O'Hara, R., Casalunovo, T., Conlin, L.K., D'Arcy, M., et al. (2009). High-resolution mapping and analysis of copy number variations in the human genome: a data resource for clinical and research applications. *Genome Res.* *19*, 1682–1690.
26. Itsara, A., Cooper, G.M., Baker, C., Girirajan, S., Li, J., Absher, D., Krauss, R.M., Myers, R.M., Ridker, P.M., Chasman, D.I., et al. (2009). Population analysis of large copy number variants and hotspots of human genetic disease. *Am. J. Hum. Genet.* *84*, 148–161.
27. Jakobsson, M., Scholz, S.W., Scheet, P., Gibbs, J.R., VanLiere, J.M., Fung, H.C., Szpiech, Z.A., Degnan, J.H., Wang, K., Guereiro, R., et al. (2008). Genotype, haplotype and copy-number variation in worldwide human populations. *Nature* *451*, 998–1003.
28. Cooper, G.M., Coe, B.P., Girirajan, S., Rosenfeld, J.A., Vu, T.H., Baker, C., Williams, C., Stalker, H., Hamid, R., Hannig, V., et al. (2011). A copy number variation morbidity map of developmental delay. *Nat. Genet.* *43*, 838–846.
29. Turleau, C., Demay, G., Cabanis, M.O., Lenoir, G., and de Grouchy, J. (1988). 6q1 monosomy: a distinctive syndrome. *Clin. Genet.* *34*, 38–42.
30. Van Esch, H., Rosser, E.M., Janssens, S., Van Ingelghem, I., Loeys, B., and Menten, B. (2010). Developmental delay and connective tissue disorder in four patients sharing a common microdeletion at 6q13-14. *J. Med. Genet.* *47*, 717–720.
31. Wentzel, C., Lynch, S.A., Stattin, E.L., Sharkey, F.H., Annerén, G., and Thuresson, A.C. (2010). Interstitial deletions at 6q14.1-q15 associated with obesity, developmental delay and a distinct clinical phenotype. *Mol. Syndromol.* *1*, 75–81.
32. Lowry, R.B., Chernos, J.E., Connelly, M.S., and Wyse, J.P. (2013). Interstitial deletions at 6q14.1q15 associated with developmental delay and a marfanoid phenotype. *Mol. Syndromol.* *4*, 280–284.
33. Carroll, P., Renoncourt, Y., Gayet, O., De Bovis, B., and Alonso, S. (2001). Sorting nexin-14, a gene expressed in motoneurons trapped by an in vitro preselection method. *Dev. Dyn.* *221*, 431–442.
34. Trabzuni, D., Ryten, M., Walker, R., Smith, C., Imran, S., Ramasamy, A., Weale, M.E., and Hardy, J. (2011). Quality control parameters on a large dataset of regionally dissected human

- control brains for whole genome expression studies. *J. Neurochem.* *119*, 275–282.
35. Kang, H.J., Kawasawa, Y.I., Cheng, F., Zhu, Y., Xu, X., Li, M., Sousa, A.M., Pletikos, M., Meyer, K.A., Sedmak, G., et al. (2011). Spatio-temporal transcriptome of the human brain. *Nature* *478*, 483–489.
  36. Huang, H.-S., Yoon, B.-J., Brooks, S., Bakal, R., Berrios, J., Larsen, R.S., Wallace, M.L., Han, J.E., Chung, E.H., Zylka, M.J., and Philpot, B.D. (2014). Snx14 regulates neuronal excitability, promotes synaptic transmission, and is imprinted in the brain of mice. *PLoS ONE* *9*, e98383.
  37. Teasdale, R.D., and Collins, B.M. (2012). Insights into the PX (phox-homology) domain and SNX (sorting nexin) protein families: structures, functions and roles in disease. *Biochem. J.* *441*, 39–59.
  38. Casimir, C.M., Bu-Ghanim, H.N., Rodaway, A.R., Bentley, D.L., Rowe, P., and Segal, A.W. (1991). Autosomal recessive chronic granulomatous disease caused by deletion at a dinucleotide repeat. *Proc. Natl. Acad. Sci. USA* *88*, 2753–2757.
  39. Wang, X., Zhao, Y., Zhang, X., Badie, H., Zhou, Y., Mu, Y., Loo, L.S., Cai, L., Thompson, R.C., Yang, B., et al. (2013). Loss of sorting nexin 27 contributes to excitatory synaptic dysfunction by modulating glutamate receptor recycling in Down's syndrome. *Nat. Med.* *19*, 473–480.
  40. Pangrazio, A., Fath, A., Sbardellati, A., Orchard, P.J., Kasow, K.A., Raza, J., Albayrak, C., Albayrak, D., Vanakker, O.M., De Moerloose, B., et al. (2013). SNX10 mutations define a subgroup of human autosomal recessive osteopetrosis with variable clinical severity. *J. Bone Miner. Res.* *28*, 1041–1049.
  41. Worby, C.A., and Dixon, J.E. (2002). Sorting out the cellular functions of sorting nexins. *Nat. Rev. Mol. Cell Biol.* *3*, 919–931.
  42. Zheng, B., Ma, Y.-C., Ostrom, R.S., Lavoie, C., Gill, G.N., Insel, P.A., Huang, X.-Y., and Farquhar, M.G. (2001). RGS-PX1, a GAP for Gα<sub>i</sub> and sorting nexin in vesicular trafficking. *Science* *294*, 1939–1942.
  43. Zheng, B., Lavoie, C., Tang, T.-D., Ma, P., Meerloo, T., Beas, A., and Farquhar, M.G. (2004). Regulation of epidermal growth factor receptor degradation by heterotrimeric Gα<sub>i</sub> protein. *Mol. Biol. Cell* *15*, 5538–5550.
  44. Zheng, B., Tang, T., Tang, N., Kudlicka, K., Ohtsubo, K., Ma, P., Marth, J.D., Farquhar, M.G., and Lehtonen, E. (2006). Essential role of RGS-PX1/sorting nexin 13 in mouse development and regulation of endocytosis dynamics. *Proc. Natl. Acad. Sci. USA* *103*, 16776–16781.
  45. Miller, J.A., Ding, S.L., Sunkin, S.M., Smith, K.A., Ng, L., Szafer, A., Ebbert, A., Riley, Z.L., Royall, J.J., Aiona, K., et al. (2014). Transcriptional landscape of the prenatal human brain. *Nature* *508*, 199–206.
  46. Langfelder, P., and Horvath, S. (2008). WGCNA: an R package for weighted correlation network analysis. *BMC Bioinformatics* *9*, 559.
  47. Konopka, G. (2011). Functional genomics of the brain: uncovering networks in the CNS using a systems approach. *Wiley Interdiscip. Rev. Syst. Biol. Med.* *3*, 628–648.
  48. Lee, K.M., Hwang, S.K., and Lee, J.A. (2013). Neuronal autophagy and neurodevelopmental disorders. *Exp. Neurobiol.* *22*, 133–142.
  49. Zoghbi, H.Y., and Bear, M.F. (2012). Synaptic dysfunction in neurodevelopmental disorders associated with autism and intellectual disabilities. *Cold Spring Harb. Perspect. Biol.* *4*, a009886.
  50. Ba, W., van der Raadt, J., and Nadif Kasri, N. (2013). Rho GTPase signaling at the synapse: implications for intellectual disability. *Exp. Cell Res.* *319*, 2368–2374.